Photovoltaic Solar Cells for Outdoor LiFi Communications

N. Lorriere, N. Betrancourt, M. Pasquinelli, G. Chabriel, J. Barrere, L. Escoubas, J.-L. Wu, V. Bermudez, C.M. Ruiz, J.-J. Simon

Photovoltaic Solar Cells for Outdoor LiFi Communications

N. Lorrière, N. Bétrancourt, M. Pasquinelli, G. Chabriel, J. Barrère, L. Escoubas, J.-L. Wu, V. Bermudez, C. M. Ruiz and J.-J. Simon

***Index Terms*—Visible Light Communication (VLC), LiFi, Solar modules, Solar cells, DC biased Optical - Orthogonal Frequency Division Multiplexing (DCO-OFDM), indoor/outdoor applications**

***Abstract*—Increasing demand of wireless devices contributes to radiofrequency (RF) congestion. Light Fidelity (LiFi) promises to be an interesting alternative by using the visible part of the electromagnetic spectrum instead of the RF part as nearly all existing wireless transmission systems do.**
A basic LiFi system is composed of one intensity-controlled light-emitting diode (LED) and one receiver device sensitive to very high-frequency (thus invisible to human sight) modulations of the luminous intensity. In most cases, the photoreceptor is a silicon photodiode of PIN (P-type intrinsic N-type) or APD (Avalanche photodiode) conception. Recently, a few studies suggest that photovoltaic (PV) modules could be used to implement outdoor LiFi transmissions, *i.e.*, under direct sunlight exposure.
In this paper, we propose to compare the behavior of a PV module and a commercial APD-based photodetector (without any optical lens or colored filter) for experimental LiFi transmissions on both indoor and outdoor conditions. The performance of the two solutions is quantified in terms of various frequency responses like attenuation, signal-to-noise ratio, or bit-error rate. The results show that, while the photodiode exhibits very good performance in indoor conditions, its frequency response is rapidly deteriorating when a sunlight exposure of more than 200W/m^2 is superimposed over the LiFi signal. We demonstrate that a PV module in V_{oc} (open-circuit voltage) condition still operates a LiFi transmission under additional solar illumination.

I. Introduction

The rapid and massive demand-led growth for communication frequencies created by wireless devices (from a simple remote control to automatic vehicles [1], through all coming soon Internet of Things (IoT) and smartphones) is leading to a Radio Frequency (RF) spectrum "bottleneck," increasing the difficulty of finding available bandwidth. At the same time, blue Light Emitting Diode (LED) has gained a huge interest since its discovery in 1972 until its intensity reached one candela in 1993 [2]. It will ultimately replace conventional lighting systems over the coming years.
In this context, Visible Light Communication (VLC), under standardization since 2011 [3], would offer a novel alternative to RF communications. For example, and as an application, LiFi (Light Fidelity - a term coined by Harald Haas in 2011 [4]) technology would complement the WiFi systems to remedy the lack of RF channels reusing the existing lighting infrastructure. In the context of LiFi, light is emitted by a LED and detected by a single photodetector which converts the light intensity high-frequency variations (invisible to the human eye) into an electrical signal. These kinds of systems are referred to as Intensity-Modulated/Direct-Detection (IM/DD) systems.
In IoT applications, a high data-rate is generally not required, and the use of receivers with a bandwidth of some hundreds of kHz to MHz is often sufficient [5]. In addition, the authors in [6] claim that most applications in energy management, health and security systems, only require a data rate of less than 1 Mbps. In an other hand, low power consumption and high reliability in indoor or outdoor conditions will also be required for near future VLC applications like e.g., Vehicle-to-Infrastructure (V2I) and Vehicle-to-Vehicle (V2V) [1]. We propose here to compare the performance of two kinds of LiFi photodetectors (photodiodes and PV modules) intended to optical wireless communication systems in indoor and outdoor environments.

The implementation of photodiodes (PD) as VLC photoreceivers raises a major drawback: PD-based photoreceivers face a problem of performance reduction under sunlight exposure [7], [8]. Despite this, Islim *et al.* [9], [10] showed that it was possible to establish communications under solar irradiation by using a blue LED emitter, a blue filtered APD receiver and an additional lens focusing the LED light beam towards the APD.

On the other hand, PV cells are optimized for outdoors energy harvesting, making them potential candidates for use as VLC receivers in outdoor applications. This study thus aims to check if PV modules can be used and outmatch PD's performance as VLC receivers in both indoor and outdoor conditions. Moreover, the possibility to combine energy harvesting and data communication has been already demonstrated [11], [12], highlighting the interest of PV modules for self-powered IoT device design.

Most of outdoors optical communications (called FSO for Free-Space Optical communication) use laser-emitters, and

N. Lorrière, M. Pasquinelli, L. Escoubas, C. M. Ruiz, and J.-J. Simon are with Aix Marseille Univ, Univ Toulon, CNRS, IM2NP, Marseille, France (e-mail: nominoe.lorriere@im2np.fr; marcel.pasquinelli@univ-amu.fr; ludovic.escoubas@univ-amu.fr; carmen.ruiz-herrero@im2np.fr; jean-jacques.simon@univ-amu.fr).

N. Bétrancourt was in an internship at Aix Marseille Univ, Univ Toulon, CNRS, IM2NP, Marseille, France (e-mail: nathan.betrancourt@etu.univ-amu.fr).

G. Chabriel and J. Barrère are with Univ Toulon, Aix Marseille Univ, CNRS, IM2NP, La Garde, France (e-mail: gilles.chabriel@im2np.fr; jean.barrere@im2np.fr).

J.-L. Wu and V. Bermudez are with Atsugi Research Center, Solar Frontier K.K., Atsugi, Kanagawa 243-0206, Japan (e-mail: jyh-lih.wu@solar-frontier.com; vbermudezbenito@hbku.edu.qa).

some of them use a PV receiver [13], [14], [15]. However, to the best of our knowledge, only a few publications address LED-based VLC with PV modules as receivers [16], [17], [18], [19], [20], and none shows a data communication in real outdoor conditions. This work compares experimental performance obtained by a PV-based receiver and a PD-based receiver with a large range of solar irradiation levels and without any lens or color filter to improve the strength of the information signal. The data are sent from a standard white LED light source. Note that comparison with blue-LED/blue-filter systems remains an open problem.

The remainder of the paper is structured into five sections: the following section II puts in balance physical characteristics of photodiodes and PV modules with the VLC receiver requirements. The VLC experimental setup we developed is presented in section III. Section IV compares, in indoor conditions, the frequency bandwidth of a popular photodiode-based photoreceiver (Hamamatsu APD module C12702-12) with that of a high-efficiency CIGS[a] based solar module provided by Solar Frontier company. The APD and PV performance is then evaluated in terms of gain, bandwidth, and BER in real outdoor conditions. Finally, the last Section V gives a general conclusion, including perspectives.

II. Photoreceivers electrical modelling

To operate outdoors, a VLC receiver has to detect small light variations broadcast by the emitting LED while being subject to a dominant DC illumination due to sunlight. In what follows, we review the pros and cons of using a photodiode or a PV module for VLC.

A. VLC reception by a photodiode

Currently, all VLC commercial solutions use photodiode-based devices as photoreceivers. PD are able to detect low-level light variations. This performance is due to the high quality of current microelectronics-grade silicon combined with the use of a high gain transimpedance amplifier (TZ) to obtain a voltage output ready for sampling (see Fig. 1). In addition to the amplifying effect, the TZ is designed to maintain the anode voltage at a constant level (a zero voltage in the example in Fig. 1) to ideally shunt all photocurrent I_{PH} through the feedback resistance R_f. The PD's transient capacitor, already reduced by the high reverse voltage, tends to be bypassed, enhancing the cutoff frequency of the device, which becomes (theoretically) only limited by that of the TZ.

Currently, two types of photodiodes are used for VLC applications:

- silicon PIN photodiodes: an intrinsic region is inserted between the two doped regions increasing the volume where an incident photon can generate electron-hole pairs,
- silicon avalanche photodiodes APD: a high reverse bias is applied to increase the electric field and therefore the velocity of carriers responsible for the avalanche effect.

[a]CIGS: Copper Indium Gallium Selenide - A thin-film technology of solar cells.

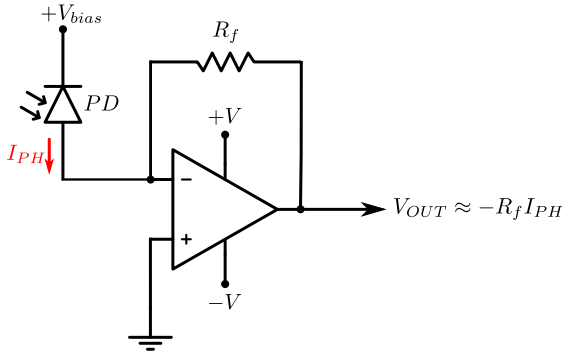

Fig. 1. PD - TZ basic circuit (photoconductive mode)

Due to the avalanche phenomenon, APD exhibits a higher photosensibility compared to a PIN photodiode. As the TZ gain decreases with decreased feedback resistor R_f (see Fig.1), a lower value of R_f conducts to a higher bandwidth[b], APD is then expected to give a higher bandwidth rather than PIN photodiodes [21].
In the literature, due to its superior quantum efficiency, one can often read that using an APD is more effective in improving the SNR than PIN diodes (see e.g. [7]), particularly at low optical powers (see [22], p.70). But it seems that this may not always be the case for high optical powers [23].

Note that the very small active areas of standard photodiodes can lead to light halo mismatch or shading effects.

One can then outline the following "benefits vs. drawbacks" for the use of a PD-based device as VLC receiver (compared to PV modules):

- Benefits:
  - high bandwidth,
  - the output voltage has a linear variation with the illumination (V_{OUT} proportional to I_{PH}, see Fig. 1),
  - the avalanche phenomenon improves detection of small light intensity variations.
- Drawbacks:
  - small detection surface,
  - the need for a very high performance amplifier circuit (high cost) *i.e.* low noise and high gain-bandwidth product.

B. VLC reception by an open-circuit PV module

Usually, PV cells are connected in series to make modules whose the open-circuit output voltage (V_{oc}) can be directly used to detect light modulations without any transimpedance amplifier or additional power supply.

1) Solar cell: The conventional one-diode electrical equivalent model of a PV [24] presented in Fig. 2 is suitable only for static (DC) signals.

The different elements of the equivalent circuit are as follows:

[b]gain-bandwidth product conservation.

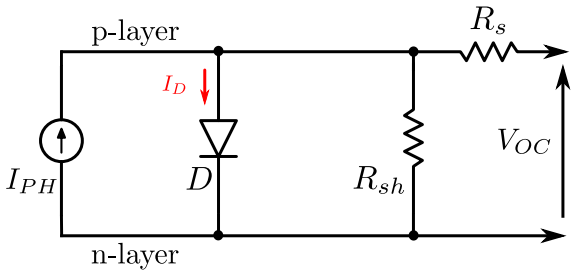

Fig. 2. Equivalent electrical circuit of a PV cell (DC) [24]

- photocurrent generator I_{PH}: the electron-hole pairs generated by light are swept away by drift in the depletion region, then collected by diffusion from the undepleted regions,
- diode D: the dark current I_D mainly corresponds to diffusion phenomena inside the forward-biased p-n junction,
- shunt resistance R_{sh}: a resistance which corresponds to leakage currents due to metallic impurities in the junction, cristal lattice defaults [25], and potential current leakages on the module edges. The corresponding resistance is generally high (several $k\Omega$)
- lumped series resistance R_s: a resistance due to busbars, contact interfaces, and semiconductors conductivity.

In the ideal case R_{sh} is taken to be near infinite then the current through R_{sh} approaches zero and consequently $I_D \approx I_{PH}$. From the Shockley diode equation, it comes, at low frequency:

$$V_{OC} = nV_T \ln\left(\frac{I_{PH}}{I_s} + 1\right), \tag{1}$$

where:

- n is the ideality factor of the junction,
- V_T is the thermal voltage (proportional to absolute temperature T),
- I_s is the reverse saturation current.

Let us consider now that the photocurrent I_{PH} involves a DC component (I_{ph}) and AC small variations (i_{ph}), with $i_{ph} \ll I_{ph}$. To represent the AC behavior of the receiver, one can replace the forward-biased diode D by its dynamic model. It embeds a dynamic resistance:

$$r_d = \frac{nV_T}{I_{ph}}, \tag{2}$$

and a dynamic capacity (diffusion capacity):

$$C_d = \frac{I_{ph}\tau}{nV_T} = \frac{\tau}{r_d}, \tag{3}$$

where the parameter τ represents the effective minority-carrier lifetime.

One obtains the linearized equivalent circuit [26] in Fig. 3 modeling the small variations of the open-circuit voltage (v_{oc}) as a function of the small variations of the photocurrent (i_{ph}). Note that this model does not take into account the possible existence of trapped charge carriers in the material structure. In [16], the wire connections are more accurately modeled by adding a small inductance (typically a few tens of nH) in the output branch of the model, *i.e.*, in series with the resistance Rs. When the PV module is highly loaded, this slightly inductive effect introduces a HF additional pole in the transfer function. It can be ignored here, given the small loads and the small bandwidths we consider in this study.

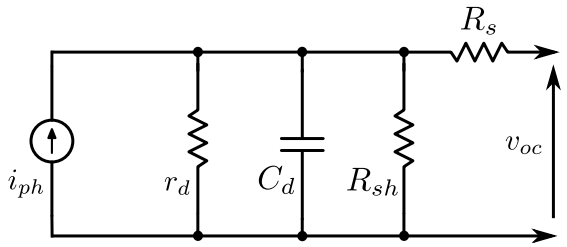

Fig. 3. Equivalent electrical circuit of a PV cell (AC small-signal linearization) [26]

With $r_d \ll R_{sh}$ and $r_d C_d = \tau$ (see (2) and (3)), the following frequency transimpedance response $T_1(f)$ is obtained for a PV cell on open-circuit conditions:

$$T_1(f) \triangleq \frac{v_{oc}^F(f)}{i_{ph}^F(f)} \approx \frac{r_d}{1 + \mathrm{j}2\pi r_d C_d f} = \frac{r_d}{1 + \mathrm{j}2\pi\tau f} = \frac{K}{1 + \mathrm{j}\frac{f}{f_c}}, \tag{4}$$

where the superscript $.^F$ denotes the Fourier transform.

The corresponding transfer function is then equivalent to that of a first-order lowpass filter whose static gain is $K = r_d$, and the -3dB cutoff frequency is $f_c = \frac{1}{2\pi\tau}$. Equation (2) shows that the gain tends to decrease with increased DC illumination and to increase with the temperature. The bandwidth is also expected to be, to a lesser extent, both temperature and injection level dependent since it is fully determined by the lifetime τ [27].

This latter result calls the following important comment: since the efficiency of a solar cell (in terms of energy harvesting) increases with the minority-carrier lifetime [28], one cannot expect to obtain a high bandwidth photoreceiver from an efficient PV cell operating in open-circuit conditions.

2) Solar module: A solar module generally corresponds to several solar cells connected in series in order to get higher output voltage.

Figure 4 represents, in the frequency domain, the small-signal equivalent circuit of a PV module built from N identical cells. To simplify, each cell is here assumed to be subjected to the same illumination. Moreover, the complex impedance $Z_{eq}(f)$ is equivalent to that of the two dynamic parameters (r_d and C_d) of one cell connected in parallel: $Z_{eq}(f) = r_d/(1 + \mathrm{j}2\pi\tau f)$.

Considering that $v_{oc}^F(f) = NZ_{eq}(f)i_{ph}^F(f)$, the V_{OC} frequency response $T_N(f)$ of a N cells PV module is given by:

$$T_N(f) = NZ_{eq}(f) = \frac{Nr_d}{1 + \mathrm{j}2\pi\tau f}. \tag{5}$$

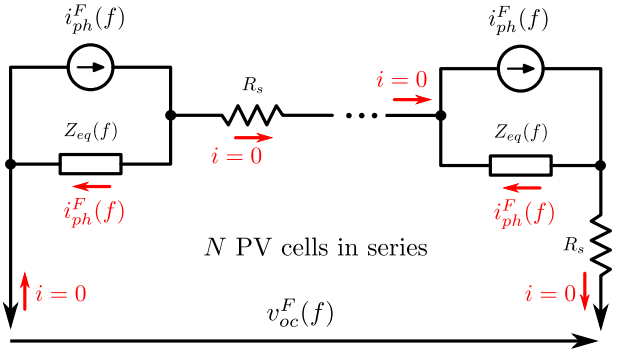

Fig. 4. Equivalent electrical circuit of a PV module (AC small-signal linearisation)

Equation (5) is similar to that of a single solar cell (same order and same cutoff frequency) except for the static gain, which is multiplied by the number N of cells.

As a conclusion, an analysis of the "benefits vs. drawbacks" for the use of a PV-based device as VLC passive receiver can be summed up as follows.

- Benefits:
  - self-powered (neutral energy) LiFi receiver, allowing both energy harvesting and LiFi signals detection,
  - wide detection surface, allowing both to resist to a partial shading and to get an angular acceptance wider than with photodiodes.
- Drawbacks:
  - low bandwidth, due to the time constant $\tau = r_d C_d$ which is not bypassed here (V_{oc} condition) as in the case for photodiodes by means of a TZ,
  - limited range of the received light variations: according to the logarithmic variation of V_{OC} as a function of the illumination (equation 1), the received light variations i_{ph} must remain reasonably low to maintain a near-linear relation with the output voltage variation v_{oc}.

III. Experimental Setup Description

A. LiFi test bench

The LiFi test bench developed at IM2NP is presented in Fig. 5. All indoor LiFi characterizations are performed in a dark Faraday cage protecting the measurements from perturbing lights or RF radiations.

In this set-up, the emitting LED sends a sequence of OFDM (orthogonal frequency division multiplexing) symbols. OFDM signals are widely used in wireless digital transmissions due to their optimal spectral efficiency and their ability to deal with non-flat transmission channels (as is the case here). For optical systems, several OFDM versions exist [29], [30]. The light intensity modulation chosen in this work is a DC biased optical (DCO) OFDM, with a cyclic prefix (CP). CP duration has to be chosen greater than or equal to the channel impulse response duration in order to guarantee steady-state channel measurements (e.g., about 3.3τ for a PV module). These CP-DCO-OFDM signals have here a dual function: they allow the estimation of various spectral characteristics (gain, SNR, noise PSD...) of the receiver and, therefore, to simultaneously evaluate the transmission performance *e.g.* in term of bit-error rate (BER). Moreover, the very short measurement duration (40 milliseconds), is here particularly suitable for outdoor experiments, ensuring that the sunlight exposure remains at an almost constant level.

In this study, data are broadcast by a 24 blue LED module overcoated with a large phosphor layer. This module is referenced as Philips Lumileds Luxeon CoB Core Range G3 L2C5-40901202E0900 and we have measured a cutoff frequency of 1.03 MHz. At the receiving end, the APD Hamamatsu photodetector is directly connected by a coax cable to the digital oscilloscope for analog-to-digital conversion (ADC) while high-frequency point probes are used with the Solar Frontier PV module (Fig. 5 and Fig. 12).

A complete description of the bench (hardware and signals) can be found in [31].

B. Description of the transmission parameters

The transmission parameters used to compare the performance of the two receivers are given in Table I, where a) summarizes the CP-DCO-OFDM signal characteristics, and b) gives the hardware parameters. Note that the maximum frequency F_{max} of the outdoor use signal is chosen lower than the indoor use one because of the noise.

TABLE I
Transmission Parameters

a) CP-DCO-OFDM signal parameters	
Number of sent symbols N_s	96
Oversampling factor	10
Number of payload subcarriers N_c	255
Guard interval size (S_{GI})	1 OFDM symbol
Complex data constellation map	4-QAM (M = 4)
Minimum frequency F_{min}	4.88 kHz out / 195 kHz in
Maximum frequency F_{max}	1.25 MHz out / 5 MHz in
b) Hardware parameters	
T/R distance	23 cm
Luminous intensity of LED polarization	5080 lux
Maximum luminous modulation	3135 lux
AC Generator	10 Vpp
DC Generator	200 mA

With these parameters, the (maximum) data rate (DR) is given by

$$DR = \frac{F_{max}\log_2(M)}{(1+S_{GI})}, \tag{6}$$

where M represents the modulation order and S_{GI} a fraction of the OFDM symbol duration. DR reaches 1.25 Mbps in outdoor conditions (5 Mbps indoor).

In what follows, the estimation of the photoreceivers spectral response H (see [31] for mathematical expression), and the BER (given by the number of wrong bits over the whole number of bits sent) will be measured under different irradiation levels.

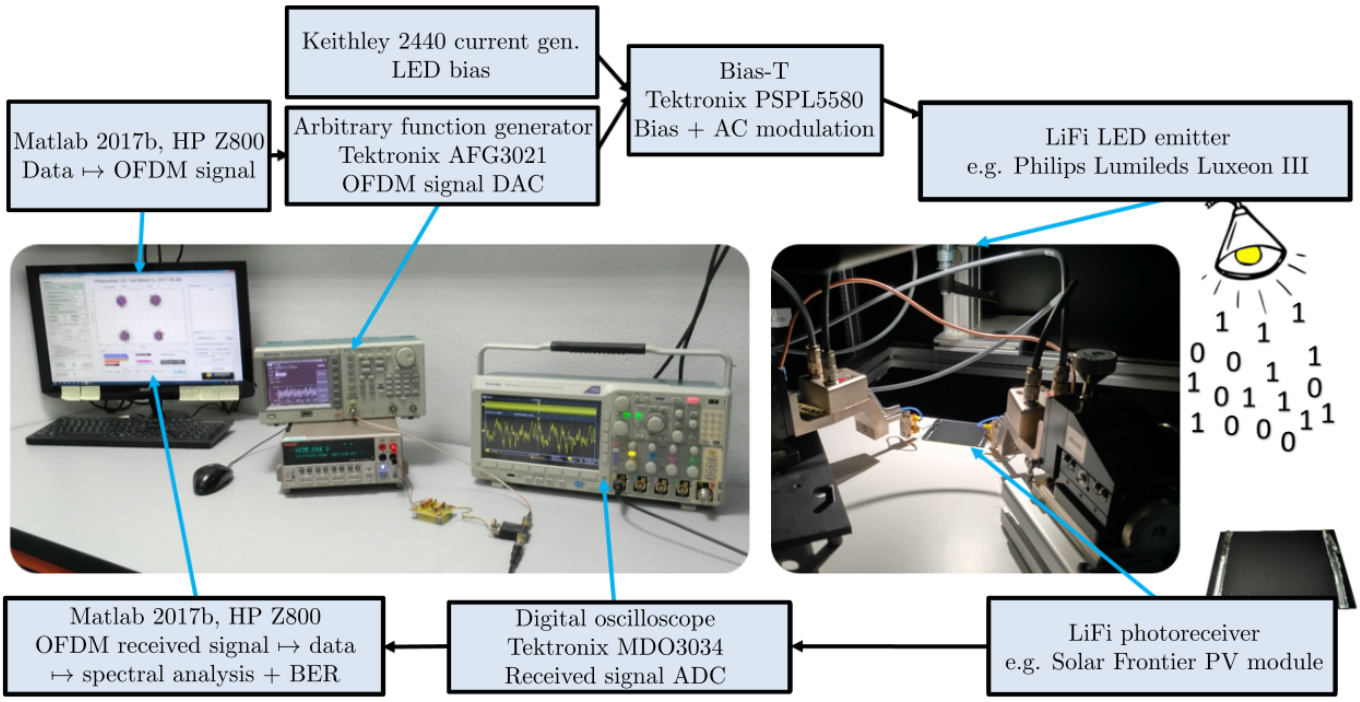

Fig. 5. IM2NP's LiFi test bench (indoor condition)

The frequency BER function (*i.e.* BER(f)) is here defined as the ratio between the number of wrong bits N_{wb} (the number of misallocated bits) received at frequency f, and the corresponding number of transferred bits N_{tb}. The BER(f) frequency resolution is the lowest quantifiable value of BER(f), which is to say corresponding to a single misallocated bit ($N_{wb} = 1$). The BER(f) frequency resolution is given by $\frac{1}{N_{tb}} = \frac{1}{N_s \log_2(M)}$. It is equal to $\frac{1}{96\times2} = 5.10^{-3}$ for our measurements. For the chosen modulation, better resolutions and smoother frequency BER functions could be reached by increasing the number of symbols N_s (*i.e.*, the measurement duration). Here we decided to set the measurement duration to 40 ms ($40\text{ms} = (1 + S_{GI})N_s F_{min}^{-1}$ where S_{GI},N_s and F_{min} values are taken from table I) ensuring the solar irradiation stability.

C. Receiver devices description

The avalanche photodiode (APD) tested here is a "Hamamatsu APD Module C12702-12". As shown in Fig. 6, the emission spectrum of the LED is fully covered by the spectral sensitivity range of the Hamamatsu APD [32]. The emission spectra of the LED (continuous blue line[c]) and sun (dashed green line[d]) correspond to the integral of their spectral irradiance on the APD active surface. The flat spectral response H_{APD} for the light intensity modulation between 10kHz and 20MHz of this APD [32] allows the calibration of the transmitting device (LED and BiasT).

[c]measurement obtained from a VISO BaseSpion goniophotometer.

[d]AM1.5 for Air Mass 1.5 is the most common standard of solar spectral irradiance utilized to quantify the performance of solar cells on earth. It is roughly valid for mid-latitude positions on earth. The ASTM G-173 standard [33] defines it.

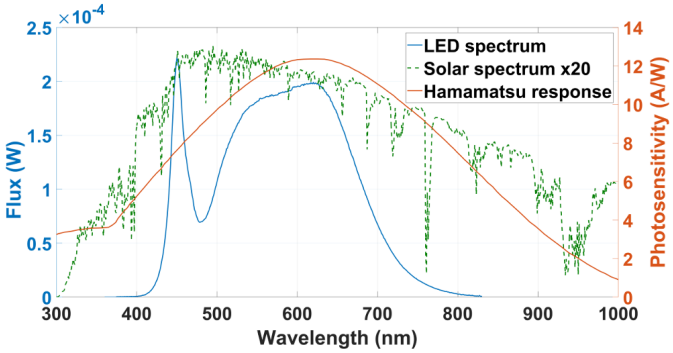

Fig. 6. Hamamatsu APD spectral response (DataSheet [32]) compared to flux received by the photodiode, provided by the LED (IM2NP measurement) and the sun.

A first measurement of the transfer function $H_{cal}(f)$ for the whole bench, including LED, Bias-T and Hamamatsu APD is performed indoor (in a darkroom), for frequencies f taken between 40 kHz and 5 MHz:

$$H_{cal}(f) = H_{LED}(f)H_{BiasT}(f)H_{APD}$$

In these conditions, the shape of $H_{cal}(f)$ is due to the LED and the BiasT. $H_{cal}(f)$ can then be used to compensate for the LED and BiasT offset in the raw transfer function measurement of any other photoreceivers $H_{raw}(f)$. Thus, the calibrated transfer function of any receivers $H_{rec}(f)$ is given by

$$H_{rec}(f) = \frac{H_{raw}(f)}{H_{cal}(f)}$$
$$\text{or} \quad H_{rec\,[dB]}(f) = H_{raw\,[dB]}(f) - H_{cal\,[dB]}(f),$$

with $H_{[dB]} = 20\log_{10}(H)$ and $40kHz \leq f \leq 5MHz$.

The PV module (provided by Solar Frontier company) is composed of 13 CIGS cells with an anti-reflecting coating. The I(V) curve on AM1.5 condition is represented in Fig. 7. Other intrinsic characteristics and useful static parameters are listed in Table II.

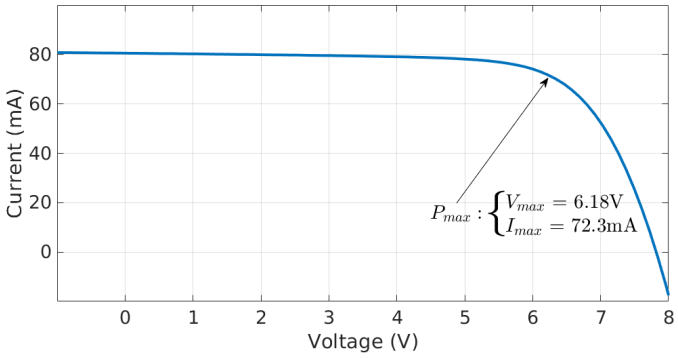

Fig. 7. Solar Frontier PV module I(V) curve (measurements from Solar Frontier company)

TABLE II
SOLAR FRONTIER PV MODULE CHARACTERISTICS

Number of cells	13
Short circuit current (mA)	80.5
Open circuit voltage (V)	7.82
Fill Factor (%)	70.96
Area (cm^2)	26.05
Current density at short circuit (mA/cm^2)	3.09
Series resistance (Ω)	12.51
Shunt resistance (Ω)	3694.70
Efficiency (%)	17.15

Similar to the APD device, Fig. 8 shows that both LED and solar spectrum are within the spectral sensibility range of the Solar Frontier PV module. The scale differences of the blue curves in Fig. 6 and Fig. 8 are due, first, to the differences between the receiver's active areas, and also, to the inhomogeneity of the LED radiation pattern. The sun power irradiation received on a photoreceiver varies as a direct function of its area. Due to the directivity of its radiation pattern, it is not true for the LED: the PV photoreceiver having a large surface, the power received from the LED is concentrated in its central area (halo) while it remains homogeneously distributed over the small area of the APD. It follows that the PV module receives 14.6% of the LED power on 26.05 cm^2 since the APD receives 1.7% of the LED power on 7.1 mm^2 [e]. Thus, for the same power emitted from the LED, the power received per unit area is 48 times higher for the APD than for the PV. Considering that the solar power received per unit area is the same for both receivers, the LED-power to the sun-power ratio (could be interpreted as some kind of SNR) confers an advantage to the APD.

[e]these values are deducted from the LED radiation pattern obtained with our VISO BaseSpion goniophotometer.

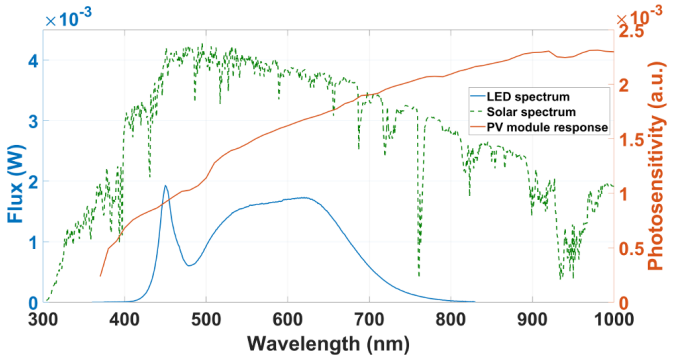

Fig. 8. Solar Frontier PV module spectral response (IM2NP measurement) compared to flux received by the PV module, provided by the LED and the sun.

The PV module spectral response presented in Fig. 8 is provided by our homemade testbench. The spectral response is measured only over a surface area of about $1mm^2$, leading to an arbitrary unit scale.

Solar Frontier PV module is used as a passive receptor, and its response is obtained from the V_{oc} variations measurements. The amplitude of input variations is bounded such that the small-signal linearized model of Fig. 3 is still valid, allowing us to extract the linear response between the CP-DCO-OFDM input signal and the output of the PV module. Within the illumination range considered, it can be verified in Fig. 9, the linear relation between the illumination level of our Arbitrary Function Generator (AFG) and the v_{oc} of the module.

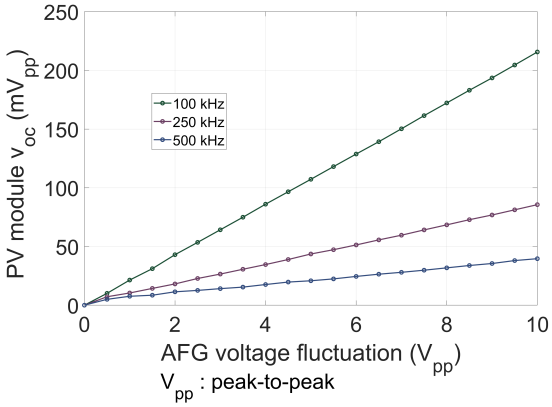

Fig. 9. Linear relation between the AFG illumination level and the PV module V_{oc} fluctuation

IV. INDOOR AND OUTDOOR RESULTS

A. Indoor measurements

The first result in Fig. 10 is a comparison of the Bode diagrams obtained for both PV and APD modules[f].

Since the output gain depends on various parameters (received light intensity, surface of the receiver, Hamamatsu module TZ gain...), only the relative voltage values of

[f]All frequency responses (gain) are obtained using the calibration step as described in section III-C.

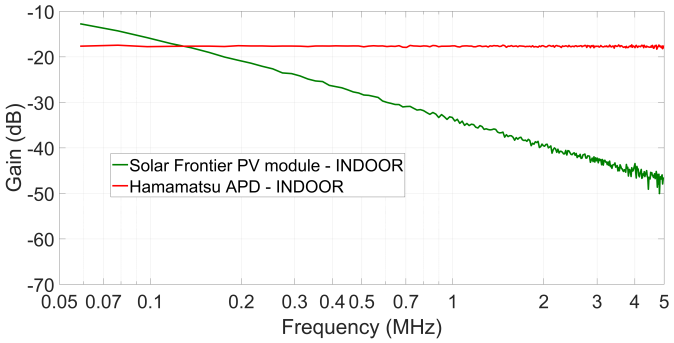

Fig. 10. Frequency response in indoor condition

the output are relevant. One can see in Fig. 10 that the photodiode presents a flat response (due to the pre-processing calibration step) while the PV module exhibits a decreasing slope of -20dB/dec in the 50kHz-5MHz frequency range. This behavior is typical of a first-order low pass filter and can be modeled by the RC electrical equivalent circuit given on Fig. 3, and for which the measured frequency range exceeds the -3dB cutoff frequency.

Fig. 11 presents the BER of our LiFi communication using the PV module then the photodiode. According to [9] and [34], the maximum admissible value for a raw BER ensuring an error-free communication (after using error correction codes) is given by 10^{-3}. As indicated in subsection III-B, a single misallocated bit leads to BER$(f) = 5.10^{-3}$ close to the admissible maximum value 1.10^{-3}. Consequently, the maximum frequency for an error-free communication will be deduced from the null BER(f) frequency range.

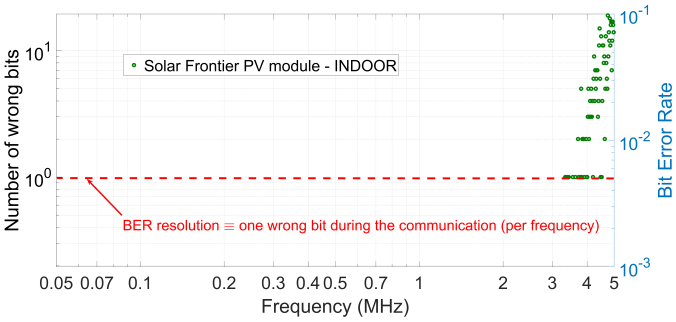

Fig. 11. BER evolution of the PV module for frequencies until 5 MHz

The data received by the Hamamatsu APD are fully recovered on the frequency range[g] of Fig. 11 while the green dots show that with the Solar Frontier module, errors occur from 3.3 MHz, whose the number increases with the frequency. This is due to the gain-loss previously observed for high frequencies.

B. Outdoor measurements

The outdoor measurements were performed in front of the IM2NP laboratory premises in the city of Marseille

[g]for higher frequencies, the measurements show that the cutoff frequency of the LED is less than that of the APD.

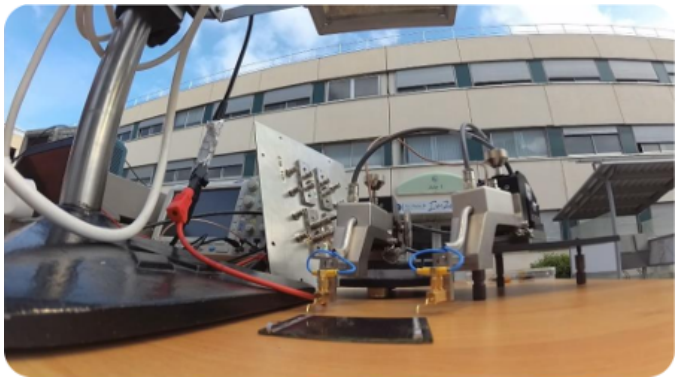

Fig. 12. Outdoor experimental setting

in France (see Fig. 12). They were performed with the parameters defined in Table I under direct sunlight exposure (without any optical system as lenses, color filters…) with different intensities according to sun elevation and ranging from 125W/m^2 to 950W/m^2, close to AM1.5 solar intensity (1000W/m^2). Note that all the exposure measurements are given with an uncertainty of $\pm$20 W/m^2.

1) Results with the APD as receiver for LiFi transmission: The frequency responses of the Hamamatsu APD obtained for various solar irradiation levels (from 125W/m^2 to 900W/m^2) and in indoor conditions (as reference) are plotted in Fig. 13.

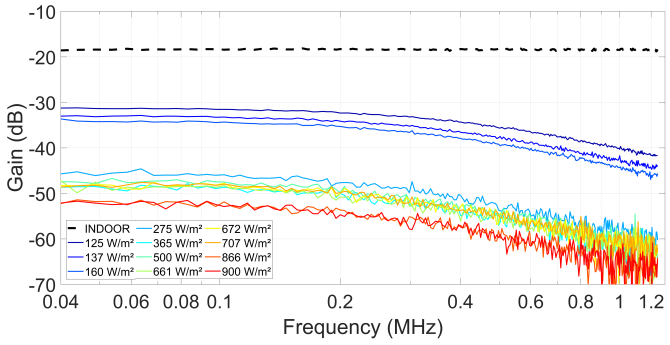

Fig. 13. APD frequency response as a function of sunlight exposure

This figure shows distinct behaviors of the APD between outdoor and indoor measurements: even under low sunlight intensities (125W/m^2), the obtained transfer function is very different from that of the Hamamatsu datasheet. A frequency cutoff appears, slightly decreasing from 0.4 to 0.2 MHz, while the gain strongly decreases, with increased sunlight intensity. According to [7], [8], this behavior could be assigned to the space charge effect (screening effect) occurring when too many free carriers are created by the solar irradiation into the semiconductor and oppose the electrical field induced by inverse applied bias voltage and the ionized dopants of the diode. This internal electric field reduction might explain both the gain reduction (reduction of the avalanche phenomenon) and the bandwidth reduction (reduction of the carrier drift speed).

At the same time, the BER also increases strongly with the solar intensity: as shown in Fig. 14, the frequency range

allowing error-free communications fades out for intensities between 160W/m^2 and 275W/m^2. Note that the three peaks

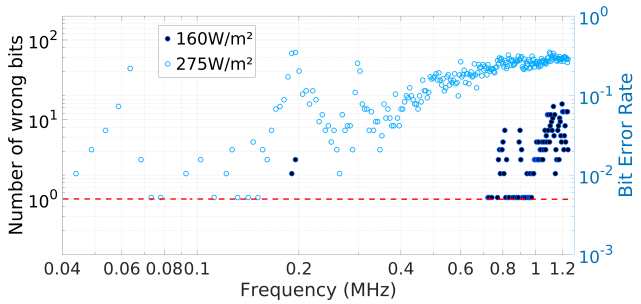

Fig. 14. APD frequency BER for two solar irradiation levels

detected around 0.06, 0.2 and 0.3 MHz in Fig. 14, are not specific to the APD but are due to intense RF perturbations as suggested by the power spectral density (PSD) of the noise estimated from the bench measurements[h] and plotted in Fig. 15. These perturbations reflect a lack of electromagnetic

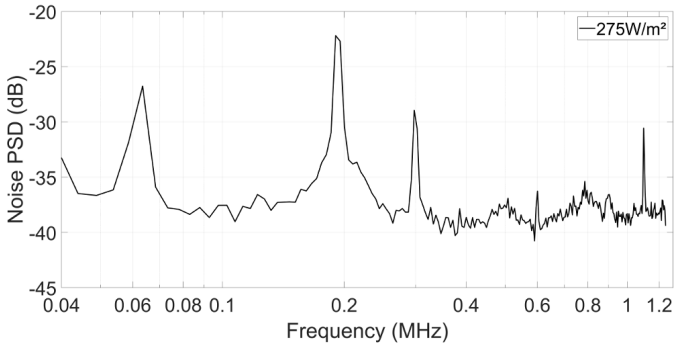

Fig. 15. APD noise power spectral density in outdoor conditions

shielding, particularly around the oscilloscope input wires.

2) Results with the solar module as receiver for LiFi transmission: The frequency responses for the PV module under different sunlight exposures are provided in Fig. 16. We can see that the gain decreases with the solar intensity, as predicted by the equation (5) where the dynamic resistance r_d is inversely related to the DC photocurrent I_{ph} (2), and thus to the solar intensity. As for the APD, Fig.17 gives the frequency bit-error rate for two solar intensities (654W/m^2 and 946W/m^2). Null BER are obtained for lower intensities ensuring error-free LiFi communications. Here again, the peaks in the frequency BER curves (around 0.23MHz and 0.75MHz) betray the presence of RF perturbations. One can notice that an error-free communication is still possible until 400kHz under a very high solar illumination level (946W/m^2).

[h]The product of the emitted data and the estimation of the transfer function gives an estimate of the data received at the PV module. This represents the signal part of the measurement. The noise part is then obtained by a simple subtraction.

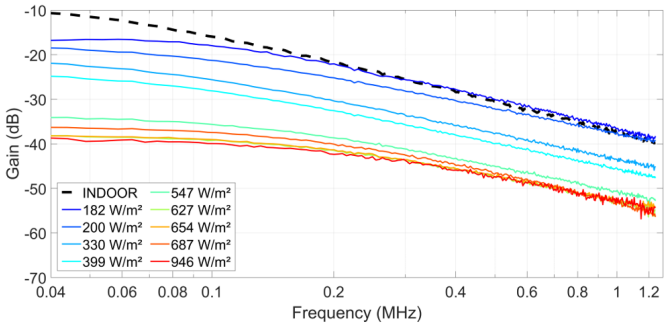

Fig. 16. PV module frequency response as a function of sunlight exposure

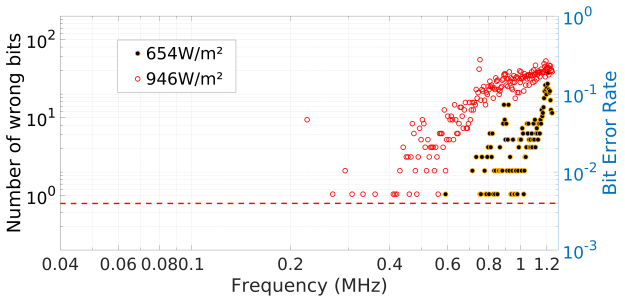

Fig. 17. PV module frequency BER for two solar illumination levels

3) Comparison of APD and PV module performance as LiFi receiver in outdoor conditions: The evolution of the total BER for the APD and the PV module as a function of sunlight intensity can be seen in Fig.18.

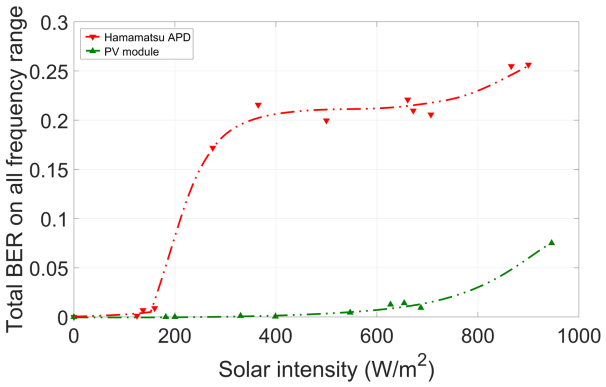

Fig. 18. Total BER as a function of sunlight exposure

In addition, since for both the solar module and the APD, the BER increases with the frequency, we define the so-called error-free maximum frequency (EFMF) to compare their suitable bandwidth for LiFi reception. Fig. 19 represents the EFMF obtained for both APD Hamamatsu and Solar Frontier PV module under different solar intensities.

These two last figures confirm the ability of the solar module to outdoor detect LiFi signals: the APD-based photodetector fails before a 200W/m^2 solar intensity level while the PV module still allows LiFi communications even

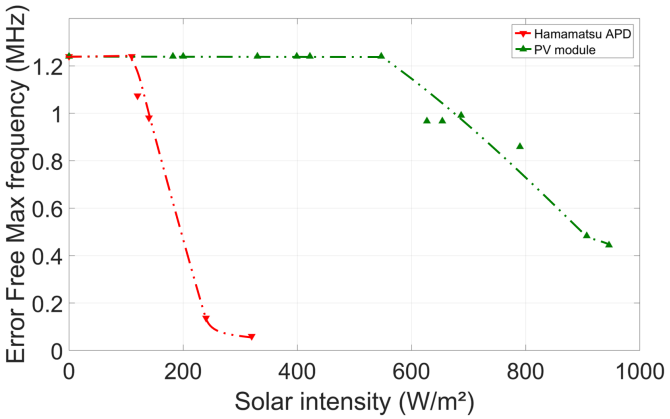

Fig. 19. Comparison of the error free maximum frequency between the hamamatsu APD and the solar module

at full sunlight exposure.

V. Conclusion and Perspectives

By means of an experimental LiFi test bench, we have compared the behavior of a PV module and a commercial APD-based photodetector for white LED LiFi transmissions in both indoor and outdoor conditions. The performance of the two solutions has been quantified in terms of frequency responses, signal-to-noise ratio and bit-error rate. Finally, the so-called error-free maximum frequency (EFMF) is introduced to quantify the limiting effect of the direct sunlight exposure on data communications. We have shown that the Hamamatsu APD-based photodetector exhibits excellent performance in indoor conditions which decreases significantly when a sunlight exposure of more than 200W/m^2 is superimposed over the LiFi signal. This behavior could be explained by a screening effect which might be confirmed by additional measurements using other photodiode-based photodetectors (APD or PIN). On the contrary, it has been demonstrated for the first time that a PV module in V_{oc} condition still operates a LiFi transmission until around 800W/m^2 which corresponds to classic outdoor lighting conditions. This shows that solar panels, as they are currently installed in solar farms, can be used as LiFi receivers. In addition, such interesting results can be extended for indoor conditions when direct or indirect sunlight illuminations are not negligible, as in the case of a system operating near a window [35].

References

[1] D.-R. Kim, S.-H. Yang, H. Kim, Y.-H. Son, and S.-K. Han, "Outdoor Visible Light Communication For Inter-Vehicle Communication Using Controller Area Network," *Proceedings of the 2012 Fourth International Conferance on Communications and Electronics (ICCE)*, pp. 31–34, 2012.

[2] S. Nakamura, T. Mukai, and M. Senoh, "Candela-class high-brightness InGaN/AlGaN double-heterostructure blue-light-emitting diodes," *Applied Physics Letters*, vol. 64, no. 13, pp. 1687–1689, 1994.

[3] Part 15.7: Short-Range Wireless Optical Communication Using Visible Light, IEEE Standard for Local and Metropolitan Area Networks, "IEEE Std.802.15.7," https://standards.ieee.org/standard/802_15_7-2011.html, 2019, accessed: 2019-01-03.

[4] H. Haas, "Wireless data from every light bulb," TEDGlobal, 2011.

[5] S. Al-Sarawa, M. Anbar, K. Alieyan, and M. Alzubaidi, "Internet of Things (IoT) Communication Protocols : Review," *Proceedings of the 2017 8th IEEE International Conference on Information Technology (ICIT)*, pp. 685–690, 2017.

[6] T. D. P. Mendes, R. Godina, E. M. G. Rodrigues, J. C. O. Matias, and J. P. S. Catalao, "Smart Home Communication Technologies and Applications: Wireless Protocol Assessment for Home Area," *Energies*, vol. 8, no. 7, pp. 7279–7311, 2015.

[7] *Hamamatsu Opto-Semiconductor Handbook*, https://www.hamamatsu.com/resources/pdf/ssd/e03_handbook_si_apd_mppc.pdf, 2019, accessed: 2020-01-16.

[8] A. Beling, X. Xie, and J. Campbell, "High-power, high-linearity photodiodes," *Optica*, vol. 3, no. 3, pp. 328–338, 2016.

[9] M. Islim and H. Haas, "An Investigation of the Solar Irradiance Effect on Visible Light Communication," *Proceedings of the 2017 IEEE 28th Annual International Symposium on Personal, Indoor, and Mobile Radio Communications (PIMRC)*, pp. 1–6, 2017.

[10] M. Islim, S. Videv, M. Safari, E. Xie, J. McKendry, E. Gu, M. Dawson, and H. Haas, "The Impact of Solar Irradiance on Visible Light Communications," *IEEE Journal of Lightwave Technology*, vol. 36, no. 12, pp. 2376–2386, 2018.

[11] Z. Wang, D. Tsonev, S. Videv, and H. Haas, "Towards Self-powered Solar Panel Receiver for Optical Wireless Communication," *Proceedings of the 2014 IEEE International Conference on Communications (ICC) - Optical Networks and Systems*, pp. 3348–3353, 2014.

[12] W.-H. Shin, S.-H. Yang, D.-H. Kwon, and S.-K. Han, "Self-reverse-biased solar panel optical receiver for simultaneous visible light communication and energy harvesting," *Optics Express*, vol. 24, no. 22, pp. A1300–A1305, 2016.

[13] J. Fakidis, S. Videv, H. Helmers, and H. Haas, "0.5-Gb/s OFDM-Based Laser Data and Power Transfer Using a GaAs Photovoltaic Cell," *IEEE Photonics Technology Letters*, vol. 30, pp. 841–844, 2018.

[14] J. de Oliveira Filho, A. Trichili, B. Ooi, M. Alouini, and K. Salama, "Towards Self-Powered Internet of Underwater Things Devices," *IEEE Communications Magazine*, pp. 1–6, 2019.

[15] S. Das, E. Poves, J. Fakidis, A. Sparks, S. Videv, and H. Haas, "Towards Energy Neutral Wireless Communications: Photovoltaic Cells to Connect Remote Areas," *Energies*, vol. 12, no. 19, pp. 1–19, 2019.

[16] Z. Wang, D. Tsonev, S. Videv, and H. Haas, "On the Design of a Solar-Panel Receiver for Optical Wireless Communications With Simultaneous Energy Harvesting," *IEEE Journal on Selected Areas in Communications*, vol. 33, no. 8, pp. 1612–1623, 2015.

[17] E. Bialic, L. Maret, and D. Kténas, "Specific innovative semi-transparent solar cell for indoor and outdoor LiFi applications," *Applied Optics*, vol. 54, no. 27, pp. 8062–8069, 2015.

[18] S.-M. Kim and J.-S. Won, "Simultaneous Reception of Visible Light Communication and Optical Energy using a Solar Cell Receiver," *Proceedings of the IEEE 2013 International Conference on ICT Convergence (ICTC)*, pp. 896–897, 2013.

[19] K. Sindhubala and B. Vijayalakshmi, "Receiver Intend to Reduce Ambient Light Noise in Visible-Light Communication using Solar Panels," *Journal of Engineering Science and Technology Review*, vol. 10, no. 1, pp. 84–90, 2017.

[20] N. Lorrière, G. Chabriel, J. Barrère, M. Pasquinelli, G. Pic, N. Vannieuwenhuyse, L. Escoubas, and J.-J. Simon, "LiFi Reception from Organic Photovoltaic Modules Subject to Additional DC Illuminations and Shading Effects," *Proceedings of the 2019 Global LiFi Congress (GLC)*, pp. 115–119, 2019.

[21] A. Prokes and O. Wilfert, "Analysis and Comparison of Various Free-Space Optical Receiver Configurations," *Proceedings of the SPIE Optics/Photonics in Security and Defence, Stockholm, Sweden*, vol. 6399, 2006.

[22] M. Azadeh, *Fiber Optics Engineering*, ser. Optical Networks. Springer US, 2009.

[23] A. Boudkhil, A. Ouzzani, and B. Soudini, "Analysis of Fundamental Photodetection Noises and Evaluation of PIN and APD Photodiodes Performances using an Optical High Debit Transmission Chain Simulated by Optisystem," *International Journal of Computer Applications (0975 –8887)*, vol. 115, no. 18, pp. 21–29, apr 2015.

[24] A. Heeger and T. Nisbet, "The solar cell - Conditions for optimum performance," *Solar Energy*, vol. 3, no. 1, pp. 12–18, 1959.

[25] T. Mambrini, "Caractérisation de panneaux solaires photovoltaïques en conditions réelles d'implantation et en fonction des différentes technologies," Ph.D. dissertation, South Paris University - Paris XI, 2014.

[26] H. Rauschenbach, *Solar Cell Array Design Handbook*. Springer Netherlands, 1980.

[27] D. J. Sandiford, "Temperature dependence of carrier lifetime in silicon," *Proceedings of the Physical Society*, vol. 71, no. 6, pp. 1002–1006, jun 1958. [Online]. Available: https://doi.org/10.1088%2F0370-1328%2F71%2F6%2F313

[28] I. Perichaud, "Gettering of impurities in solar silicon," *Solar Energy Materials & Solar Cells*, vol. 72, pp. 315–326, 2002.

[29] S. Dissanayake and J. Armstrong, "Comparison of ACO-OFDM, DCO-OFDM and ADO-OFDM in IM/DD Systems," *Journal of Lightwave Technology*, vol. 31, no. 7, pp. 1063–1072, 2013.

[30] M. Islim and H. Haas, "Modulation Techniques for Li-Fi," *ZTE Communications Special issue on Multi-Gigabit Millimeter-Wave Wireless Communications*, vol. 14, no. 2, pp. 29–40, 2016.

[31] N. Lorrière, E. Bialic, M. Pasquinelli, G. Chabriel, J. Barrère, L. Escoubas, and J.-J. Simon, "An OFDM Testbed for LiFi Performance Characterization of Photovoltaic Modules," *Proceedings of the 1st IEEE Global LiFi Congress (GLC)*, pp. 1–5, 2018.

[32] Hamamatsu website, "APD C12702 series Datasheet," https://www.hamamatsu.com/resources/pdf/ssd/c12702series_kacc1214e.pdf, 2017, accessed: 2020-01-16.

[33] *Standard Tables for Reference Solar Spectral Irradiances: Direct Normal and Hemispherical on 37° Tilted Surface*, 2012.

[34] S. Zhang, D. Tsonev, S. Videv, S. Ghosh, G. Turnbull, I. Samuel, and H. Haas, "Organic solar cells as high-speed data detectors for visible light communication," *Optica Letter*, vol. 2, no. 7, pp. 607–610, 2015.

[35] C. Reynaud, R. Clerc, P. Lechêne, M. Hébert, A. Cazier, and A. Arias, "Evaluation of indoor photovoltaic power production under directional and diffuse lighting conditions," *Solar Energy Materials and Solar Cells*, vol. 200, 2015.